Pure Appl. Geophys. 180 (2023), 3457–3475

https://doi.org/10.1007/s00024-023-03357-0

Pure and Applied Geophysics

Seismic Hazards Along the Longmen Shan Fault: Insights from Stress Transfer Between Major Earthquakes and Regional *b*-Values

Yunqiang Sun,[1] Weicheng Gong,[1] Fuquan Wei,[2] and Wen Jiang[3]

Abstract—There are two seismic gaps (Dayi seismic gap and Tianquan-Kangding seismic gap) on the Longmen Shan fault (LMSF), despite the successive occurrence of the 2008 M_w7.9 Wenchuan and 2013 M_w6.6 Lushan earthquakes. To analyze the effects of the Wenchuan and Lushan earthquakes on the LMSF (especially on seismic gaps along the LMSF) and regional seismic hazards, we calculate Coulomb stress changes caused by the Wenchuan and Lushan earthquakes based on a three-dimensional viscoelastic finite element model. Additionally, we calculate the spatial distribution of regional *b*-values based on the instrumental seismic catalog before the Wenchuan earthquake. By utilizing the inverse correlation between *b*-value and stress level, we infer the regional background stress level. The results show that regional earthquakes (including the 2008 M_w7.9 Wenchuan earthquake, 2013 M_w6.6 Lushan earthquake, 2014 M_w6.1 Kangding earthquake, 2017 M_w6.5 Jiuzhaigou earthquake, and 2022 M_w6.6 Luding earthquake) occurred in regions characterized by low *b*-values. Meanwhile, subsequent earthquakes occurred in regions where Coulomb stress changes caused by the Wenchuan and Lushan earthquakes were positive. This suggests that regions with both low *b*-values and positive Coulomb stress changes may pose higher seismic hazards. We found that there are four regions (southern Xianshuihe fault, Dongkunlun fault, northern Xiaojinhe fault, and Hanan-Qingshanwan fault) with both positive Coulomb stress changes caused by the Wenchuan and Lushan earthquakes and low *b*-values, which may indicate high stress accumulation and high seismic hazard in the future. The results also show that Coulomb stress changes caused by the Wenchuan and Lushan earthquakes increased significantly in the Dayi seismic gap ($+0.216 \sim +2.607$ MPa) and Tianquan-Kangding seismic gap ($+0.021 \sim +0.211$ MPa), while the result of the high *b*-values for the Dayi and Tianquan-Kangding seismic gaps indicate less background stress accumulation. However, with continued tectonic loading, seismic hazards on both seismic gaps should attract our attention.

Keywords: Longmen Shan fault, seismic gap, Coulomb stress changes, finite element model, *b*-value, Wenchuan earthquake.

1. Introduction

The Longmen Shan fault (LMSF) is located in the boundary between the eastern Tibetan Plateau and the South China Block (Fig. 1). It is a complex fault zone formed as a result of collectively accommodating the crustal deformation of the eastern Tibetan Plateau induced by the Indo-Asian collision. The fault zone consists of three major thrust faults: the Wenchuan-Maoxian fault, the Yingxiu-Beichuan fault, and the Guanxian-Anxian fault (Deng et al., 1994). Each of these three faults exhibits distinct thrust characteristics, with a NW dip angle of 60–70° that gradually decreases with depth, ultimately converging into a low-dip shear zone (Feng et al., 2016; Royden et al., 2008).

The LMSF has been intensely seismically active recently, with the 2008 M_w7.9 Wenchuan earthquake and the 2013 M_w6.6 Lushan earthquake occurring successively. Surface ruptures caused by the Wenchuan and Lushan earthquakes are $\sim$ 300 km of the central and northern LMSF, and $\sim$ 30 km of the southern LMSF, respectively (Chen et al., 2013). However, there are still two seismic gaps on the LMSF that have not ruptured following these two events: the Dayi seismic gap, located between the rupture zones of the Wenchuan and Lushan earthquakes, and the Tianquan-Kangding seismic gap in the southwestern LMSF (Chen et al., 2013; Pei et al., 2014; Xu et al., 2013).

It is disputed whether these two seismic gaps have the potential to generate another major earthquake. One viewpoint suggests that the Dayi and Tianquan-Kangding seismic gaps pose a high risk of future earthquakes. For example, Chen et al. (2013) analyzed the seismic moment accumulation and release

[1] College of Transportation and Civil Engineering, Fujian Agriculture and Forestry University, Fuzhou 350002, China. E-mail: yunqiang_sun@163.com

[2] Fujian Earthquake Agency, Fuzhou 350002, China.

[3] Zijin School of Geology and Mining, Fuzhou University, Fuzhou 350002, China. E-mail: jiagwen89@126.com

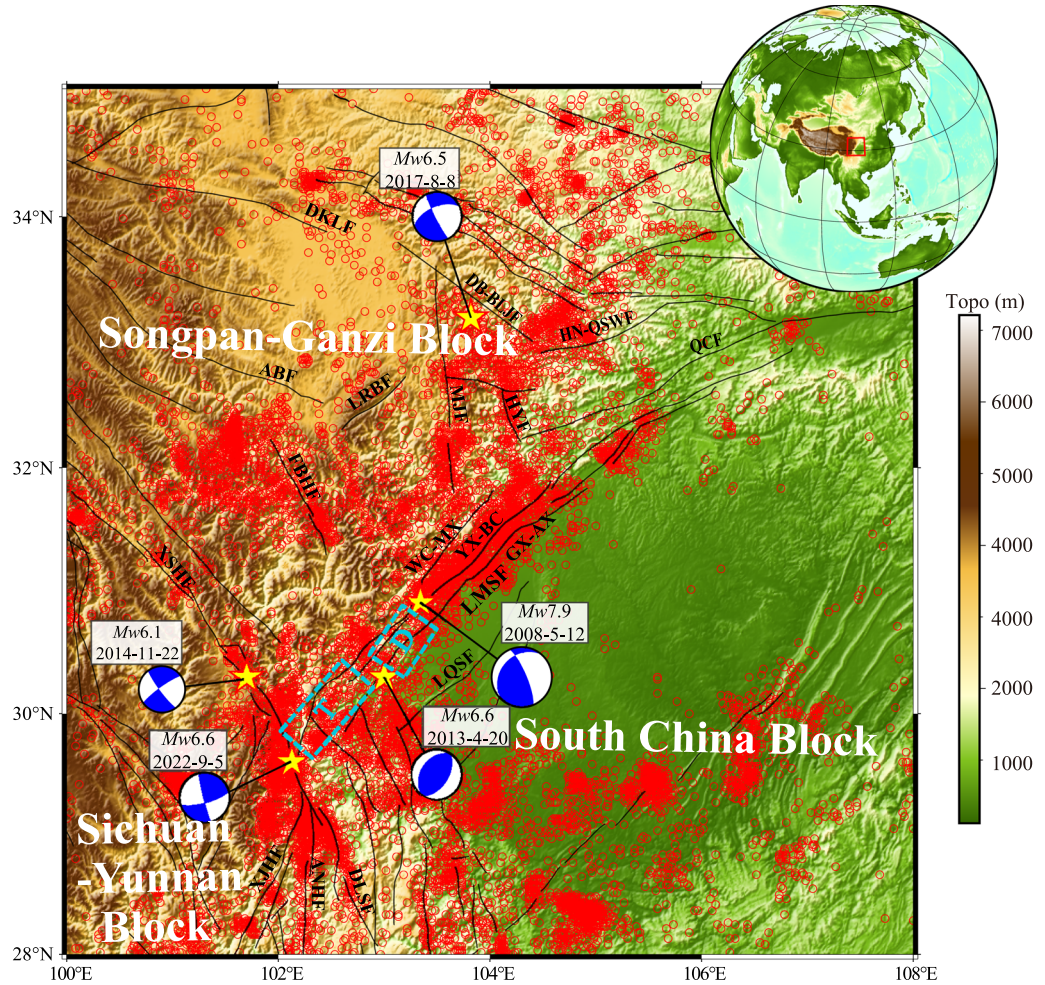

Figure 1

Tectonic background of the eastern Tibetan Plateau. The blue dashed rectangles indicate the two seismic gaps (D: Dayi seismic gap; T: Tianquan-Kangding seismic gap) along the Longmen Shan fault. Red circles are the locations of instrumental earthquakes from 1970 to 2008; data are from the China Earthquake Network Center. Blue beach balls show the focal mechanism solution of earthquakes from GCMT (http://www.globalcmt.org). *LMSF* Longmen Shan fault; *WC-MX* Wenchuan-Maoxian fault; *YX-BC* Yingxiu-Beichuan fault; *GX-AX* Guanxian-Anxian fault; *MJF* Minjiang fault; *XSHF* Xianshuihe fault; *LQSF* Longquan Shan fault; *FBHF* Fubianhe fault; *DKLF* Dongkunlun fault; *HYF* Huya fault; *QCF* Qingchuan fault; *ABF* Aba fault; *LRBF* Longriba fault; *DB-BLJF* Diebu-Bailongjiang fault; *HN-QSWF* Hanan-Qingshanwan fault; *XJHF* Xiaojinhe fault; *DLSF* Daliang Shan fault; *ANHF* Anninghe fault

in the southwestern LMSF and indicated that both the Dayi and Tianquan-Kangding seismic gaps have a high potential for future earthquakes with magnitudes of M_w6.8 and M_w7.2, respectively. This viewpoint has been verified by in situ stress state (Li et al., 2022), fault locking (Li et al., 2023), and Coulomb stress changes (Guo et al., 2020; Liu et al., 2018; Toda et al., 2008). However, some other studies such as seismic tomography (Pei et al., 2014), global positioning system (GPS)-derived fault coupling (Li et al., 2018), and paleo-earthquakes (Dong et al., 2017) are to the contrary.

Determining the stress states in a region is crucial for evaluating seismic hazards. For example, following the 2008 Wenchuan earthquake, multiple scholars have calculated Coulomb stress changes

(Guo et al., 2020; Liang et al., 2018; Liu et al., 2018; Parsons et al., 2008; Toda et al., 2008; Xu et al., 2013, 2020; Zhang et al., 2010) and found that the event has changed the regional stress field significantly. It is noteworthy that the 2013 M_w6.6 Lushan earthquake that occurred in the region with Coulomb stress changes surpassed 0.01 MPa. However, studies also show that some subsequent earthquakes occurred in regions where Coulomb stress changes caused by preceding earthquakes were negative (Gkarlaouni et al., 2008; Luo & Liu, 2018).

Compared with the background stress that has already accumulated on faults, Coulomb stress changes caused by earthquakes are a relatively small perturbation (Luo & Liu, 2018; Sun et al., 2020). Thus, a comprehensive analysis of full stress evolution on faults is crucial for further assessing the regional seismic hazards. However, determining the magnitude of regional stress remains challenging to date (Shi et al., 2018). Though Li et al. (2022) arranged two boreholes (1000 and 500 m deep) to carry out hydraulic fracturing in situ stress measurements in the Dayi seismic gap; the depth of the borehole is relatively small compared with the focal depth of regional earthquakes.

While it is still difficult to quantify the magnitude of regional stress, studies have shown that seismic *b*-values obtained from the Gutenberg–Richter (G–R) relation (Gutenberg & Richter, 1944) can provide insights into regional stress states. A lower *b*-value indicates a higher stress level, while a higher *b*-value indicates a lower stress level in a region (Dong et al., 2022; Scholz, 1968, 2015).

In this study, we establish a three-dimensional (3D) viscoelastic finite element model in the eastern Tibetan Plateau, and calculate the Coulomb stress changes caused by the Wenchuan and Lushan earthquakes. Additionally, we calculate the spatial distribution of the regional *b*-values based on the instrumental seismic catalog before the Wenchuan earthquake, and infer the regional background stress level according to the inverse correlation between the *b*-value and stress level. Finally, we analyze the regional seismic hazards by combining the results of Coulomb stress changes and regional *b*-values.

2. Finite Element Model

2.1. Model Setup

We establish a 3D finite element model of the eastern Tibetan Plateau. Figure 2 shows the mesh of the finite element model. The length and width of the model are 700 km, and the depth is 100 km. Based on the active tectonic block hypothesis (Deng et al., 2003; Shao et al., 2022), the model is horizontally divided into three blocks: South China Block, Songpan-Ganzi Block, and Sichuan-Yunnan Block (Fig. 2).

The model consists of two rheological layers at depth: the elastic upper crust, and the viscoelastic middle-lower crust and upper mantle layer. The elastic upper crust (seismogenic layer) of the model is set to be 20 km since most earthquakes in this region occur within the depth of 20 km (Shen et al., 2009; Xu et al., 2009; Zhang et al., 2010). Results of receiver function analysis indicate that the crustal thickness of the eastern Tibetan Plateau is about 50–70 km, and the crustal thickness of the Sichuan Basin is about 35–50 km (Bao et al., 2020; Gao et al., 2022; Wang et al., 2023). Thus, the layered model of the South China Block consists of the upper crust (0–20 km), middle-lower crust (20–50 km), and upper mantle (50–100 km), while the Songpan-Ganzi and Sichuan-Yunnan Blocks consist of upper crust (0–20 km), middle-lower crust (20–60 km), and upper mantle (60–100 km) (Table 1).

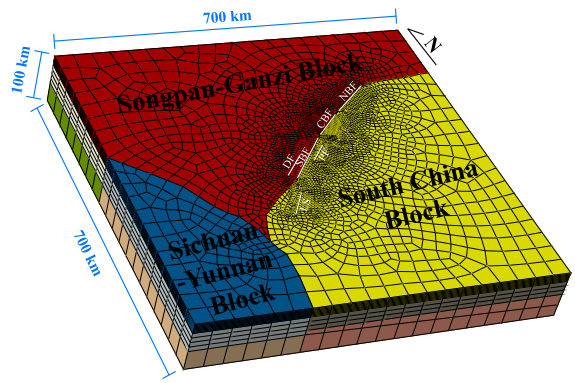

Figure 2
Three-dimensional finite element model of the eastern Tibetan Plateau

Table 1

Material parameters of the finite element model

Block	Depth (km)	P-wave velocity $V_p(km/s)$	S-wave velocity $V_S(km/s)$	Density ρ (kg/m^3)	Poisson's ratio v	Young's modulus E (Pa)
South China Block	0–20	6.10	3.60	2740	0.23	8.76×10^{10}
	20–50	6.66	3.95	2870	0.23	1.10×10^{11}
	50–100	8.04	4.70	3310	0.24	1.81×10^{11}
Songpan-Ganzi Block	0–20	6.10	3.25	2740	0.30	7.54×10^{10}
	20–60	6.65	3.40	2870	0.32	8.78×10^{10}
	60–100	8.00	4.30	3300	0.30	1.58×10^{11}
Sichuan-Yunnan Block	0–20	5.50	3.30	2740	0.22	7.27×10^{10}
	20–60	6.02	3.65	2860	0.21	9.22×10^{10}
	60–100	8.02	4.65	3300	0.25	1.78×10^{11}

According to the regional velocity and density structures from previous studies (https://igppweb.ucsd.edu/~gabi/crust1.html; Bao et al., 2020; Gao et al., 2022; Wang et al., 2023), we calculate Young's modulus (E) and Poisson's ratio (υ) of each block in the study area by using the following equations:

$$E = \frac{V_S^2 \rho (3V_p^2 - 4V_S^2)}{V_p^2 - V_S^2}, \quad (1)$$

$$\upsilon = \frac{V_p^2 - 2V_S^2}{2(V_p^2 - V_S^2)}, \quad (2)$$

where ρ is the mean density, V_S is the S-wave velocity, and V_P is the P-wave velocity.

The four lateral boundaries of the model are fixed in the normal direction and free in the tangential direction. The bottom boundary is free to move horizontally and fixed vertically, and the upper surface of the model is free.

2.2. Co-seismic Slip Model of Earthquakes

After the Wenchuan earthquake, researchers have used teleseismic waveforms, high-resolution GPS observations, and other data to invert the co-seismic slip distribution of the earthquake. For example, Ji (2008) derived a single fault plane (strike: 229°; dip: 33°) with a length of 298 km and a width of 20 km through the analysis of Global Seismic Network broadband waveforms (Fig. 3a). Wang et al. (2008) constructed a double-listric finite fault model and reconstructed the source rupture process by combined inverting the teleseismic waveforms and near-field co-seismic displacements (Fig. 3b). Wang et al. (2011) inverted a refined co-seismic slip model (Fig. 3c) with a 60 km sub-horizontal décollement fault beneath the LMSF based on GPS, InSAR, and leveling data. Fielding et al. (2013) integrated teleseismic waveform data, geodetic data (GPS), and remote sensing data (InSAR and SAR) to invert the co-seismic slip model, and produced a five-stage model of the Wenchuan earthquake (Fig. 3d). These models share a common feature of showing two maximum slip regions beneath the Beichuan and Yingxiu cities, which were heavily damaged. However, due to variations in fault geometry, observation data, and inversion strategies, there are differences in the details of these models. Thus, this study utilizes these four co-seismic slip models (Fig. 3) to calculate the co-seismic deformation of the Wenchuan earthquake.

In contrast to the Wenchuan earthquake, the influence of different rupture models of the Lushan earthquake is not significant. Therefore, we have employed the co-seismic slip model of the Lushan earthquake as proposed by Liu et al. (2013) in this study.

We then incorporated the rupture geometries and the co-seismic slip distribution of the Wenchuan and Lushan earthquakes (Fig. 3) into the finite element model (Fig. 2) with the split-node technique (Melosh & Raefsky, 1981).

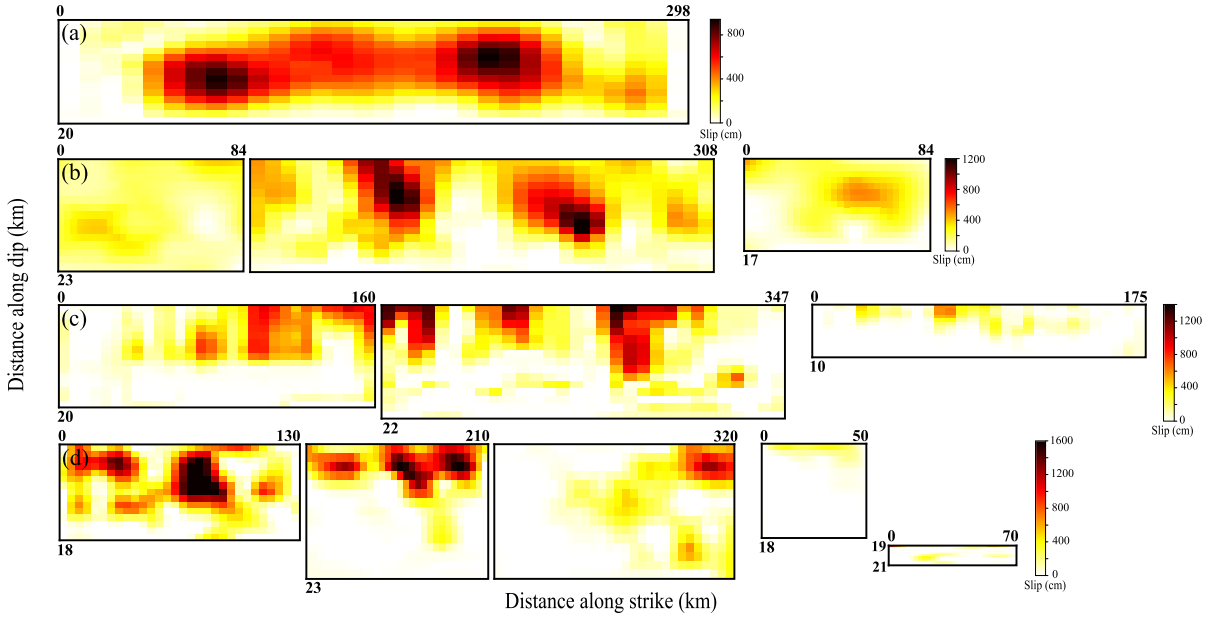

Figure 3
Co-seismic slip distributions of the rupture models for the Wenchuan earthquake. **a–d** Slip models developed by Ji (2008), Wang et al. (2008), Wang et al. (2011), and Fielding et al. (2013), respectively

2.3. Constitutive Equations

The constitutive equation of Maxwell viscoelasticity can be described as follows:

$$\dot{\varepsilon} = D^{-1}\dot{\sigma} + S\sigma, \tag{3}$$

where $\dot{\varepsilon} = \left[\dot{\varepsilon}_{xx}, \dot{\varepsilon}_{yy}, \dot{\varepsilon}_{zz}, \dot{\gamma}_{yz}, \dot{\gamma}_{xz}, \dot{\gamma}_{xy}\right]^T$, $\sigma = \left[\sigma_{xx}, \sigma_{yy}, \sigma_{zz}, \sigma_{yz}, \sigma_{xz}, \sigma_{xy}\right]^T$. D^{-1}, and S are the material matrices related to elastic and viscous deformation, respectively.

$$\mathrm{D}^{-1} = \begin{bmatrix} \frac{1}{E} & -\frac{v}{E} & -\frac{v}{E} & 0 & 0 & 0 \\ -\frac{v}{E} & \frac{1}{E} & -\frac{v}{E} & 0 & 0 & 0 \\ -\frac{v}{E} & -\frac{v}{E} & \frac{1}{E} & 0 & 0 & 0 \\ 0 & 0 & 0 & \frac{2(1+v)}{E} & 0 & 0 \\ 0 & 0 & 0 & 0 & \frac{2(1+v)}{E} & 0 \\ 0 & 0 & 0 & 0 & 0 & \frac{2(1+v)}{E} \end{bmatrix}, \tag{4}$$

$$S = \frac{1}{\eta}\begin{bmatrix} \frac{1}{3} & -\frac{1}{6} & -\frac{1}{6} & 0 & 0 & 0 \\ -\frac{1}{6} & \frac{1}{3} & -\frac{1}{6} & 0 & 0 & 0 \\ -\frac{1}{6} & -\frac{1}{6} & \frac{1}{3} & 0 & 0 & 0 \\ 0 & 0 & 0 & 1 & 0 & 0 \\ 0 & 0 & 0 & 0 & 1 & 0 \\ 0 & 0 & 0 & 0 & 0 & 1 \end{bmatrix}, \tag{5}$$

where E, v, and η represent Young's modulus, Poisson's ratio, and viscosity, respectively.

To discretize the above constitutive equation, we have utilized the derivative formula to transform it into a differential form under the assumption of small time steps:

$$\dot{\sigma}^t = \frac{\Delta\sigma^t}{\Delta t} = \frac{\sigma^t - \sigma^{t-\Delta t}}{\Delta t}, \tag{6}$$

$$\dot{\varepsilon}^t = \frac{\Delta\varepsilon^t}{\Delta t} = \frac{\varepsilon^t - \varepsilon^{t-\Delta t}}{\Delta t}, \tag{7}$$

Combining Eqs. (3), (6), and (7), the viscoelastic constitutive relation can be expressed as:

$$\sigma^t = \tilde{D}\varepsilon^t + \tilde{\sigma}, \tag{8}$$

where $\tilde{D} = (D^{-1} + S\Delta t)^{-1}$ and $\tilde{\sigma} = (D^{-1} + S\Delta t)^{-1} D^{-1}\sigma^{t-\Delta t} - (D^{-1} + S\Delta t)^{-1}\varepsilon^{t-\Delta t}$.

Based on the aforementioned theory, we independently developed the 3D viscoelastic finite element code to simulate co-seismic and post-seismic deformation based on the Abaqus secondary development platform. The reliability of this code has been verified (Gong et al., 2023; Sun et al., 2021).

3. Results

We calculate Coulomb stress changes caused by the Wenchuan and Lushan earthquakes and analyze stress transfer between major earthquakes. Then we calculate the spatial distribution of *b*-values based on the regional instrumental seismic catalog before the Wenchuan earthquake. Finally, we analyze regional seismic hazards by combining the stress transfer between major earthquakes and the spatial distribution of *b*-values.

3.1. Co-seismic Displacements Caused by Wenchuan Earthquake

The computation of co-seismic and post-seismic deformation is significantly influenced by the slip model of large earthquakes. Here, we employ four slip models of the Wenchuan earthquake (Fig. 3) to calculate the co-seismic surface displacements. To assess the accuracy of each model, we compare the simulated results from each model with GPS observations. The model that exhibits the closest match to the GPS observations is considered the most reliable and provides the best estimate of the actual co-seismic and post-seismic deformation.

The results demonstrate that modeled surface displacements generated by four slip models of the Wenchuan earthquake generally agree well with GPS observations in the far field (Fig. 4a–d). However, there are varying degrees of deviation near the rupture zone of the Wenchuan earthquake (Fig. 4). The difference may be attributed to various factors, including the complex deep structure of the earth and seismic rupture processes, as well as the relatively simplified model setting.

In order to further assess the differences between model results generated by the four slip models and GPS observations, we calculate the difference between model results and GPS observations. Figure 4e–h show the residual displacements (model displacements minus GPS displacements) for the four models. We also quantitatively count the residual of northward and eastward displacements between four model results and GPS observations (insets in Fig. 4e–h). The results indicate that the co-seismic slip model of the Wenchuan earthquake developed by Fielding et al. (2013) provides the best fit for horizontal surface displacements, with more than 80% samples of eastward (red line in subfigures of Fig. 4e–h illustrations) and northward (green line in subfigures of Fig. 4e–h illustrations) deviations stay within ± 3 cm. Therefore, we then conducted a follow-up study based on the co-seismic slip model developed by Fielding et al. (2013).

3.2. Rheology of Songpan-Ganzi Block Derived from the Viscoelastic Model

Due to the viscoelasticity of the middle-lower crust and upper mantle, crustal deformation continues following a large earthquake. Previous studies have deployed a series of GPS stations to monitor the post-seismic deformation (Diao et al., 2018; Wang et al., 2021, 2022), and have used these data to constrain the viscosities of the middle-lower crust and upper mantle (Diao et al., 2018; Hu et al., 2016; Shao et al., 2011; Wang et al., 2021).

Given the sparsity of GPS stations in the South China Block and the Sichuan-Yunnan Block in the model region (Fig. 6) (Wang et al., 2021), we determined the viscosities of their middle-lower crust and upper mantle based on previous studies (Shi & Cao, 2008; Sun et al., 2013). Specifically, we set the value of 1×10^{19} Pa·s and 1×10^{20} Pa·s for the middle-lower crust, of 1×10^{21} Pa·s, and 1×10^{22} Pa·s for the upper mantle in the Sichuan-Yunnan Block and the South China Block, respectively.

We then use the Maxwell viscoelastic model to simulate the time-dependent displacement and constrain the viscosities of the middle-lower crust and upper mantle in Songpan-Ganzi Block based on the post-seismic deformation data for nine years after the Wenchuan earthquake (Wang et al., 2021). We test the viscosities range from 1×10^{18} to 1×10^{20} Pa s for the middle-lower crust and from 1×10^{19} to 1×10^{21} Pa s for the upper mantle. Using a grid-search approach, we carry out a series of cases to find the optimal viscosities that fit the GPS observations best. The misfit degree of model results to GPS observations is evaluated by using the formula (Chai & Draxler, 2014):

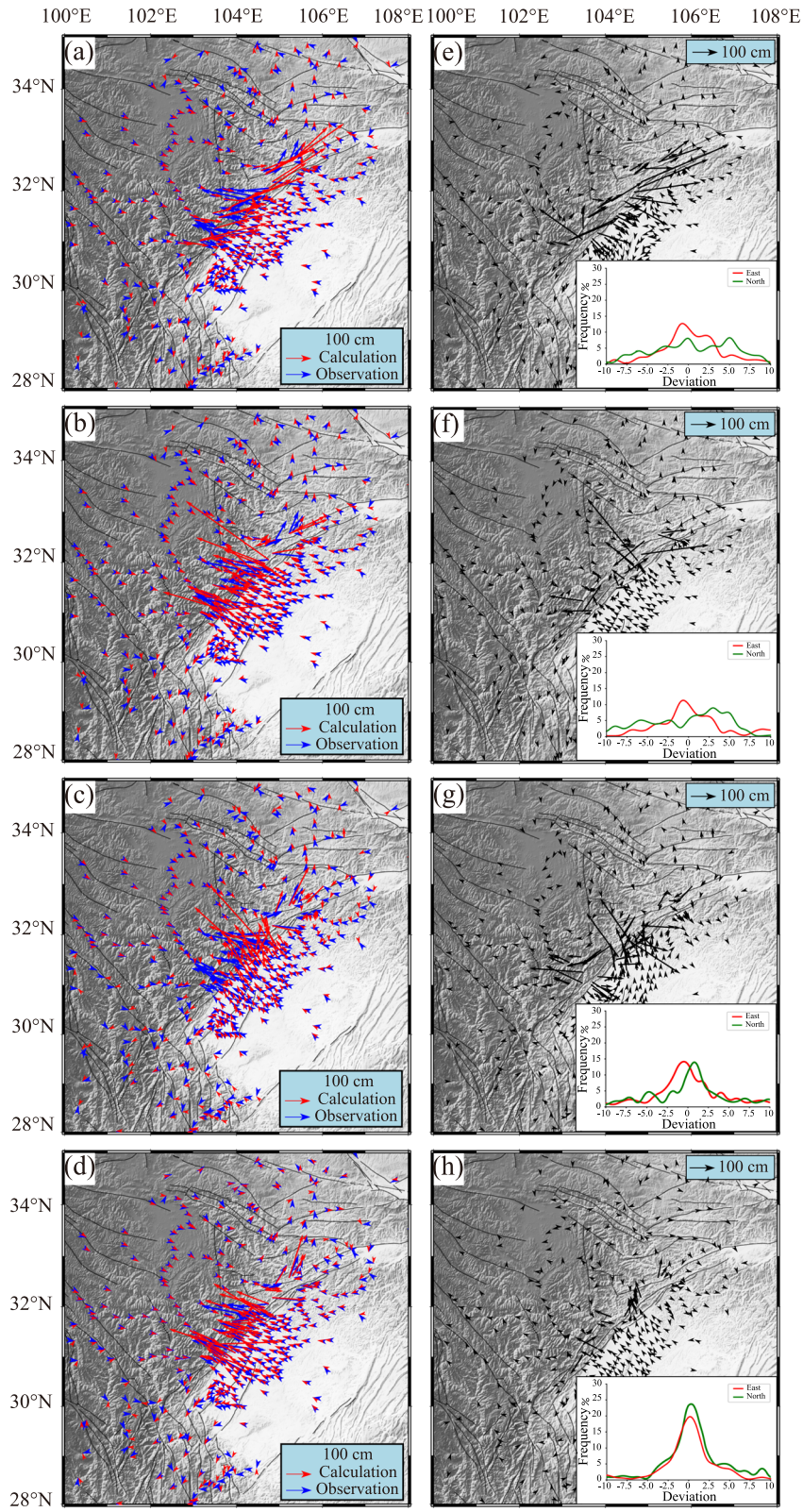
100°E
102°E
104°E
106°E
108°E
34°N
32°N
30°N
28°N
(a)
(b)
(c)
(d)
(e)
(f)
(g)
(h)
100 cm
Calculation
Observation
East
North
Frequency %
Deviation

◀Figure 4
Comparison of co-seismic surface displacements caused by the Wenchuan earthquake between model results (red arrows) and GPS observations (blue arrows) (Wang et al., 2011). **a–d** Comparison between GPS observations and the model results using the co-seismic slip model from Ji (2008), Wang et al. (2008), Wang et al. (2011), and Fielding et al. (2013), respectively. **e–h** Residual displacements between model results of the corresponding models and GPS observations. Insets in **e–f** show the corresponding distribution of residual displacements (both northward displacements and eastward displacements)

$$\mathrm{RMSE} = \sum_{i=1}^{N} \sqrt{\left[\frac{(x_i - x_i^{GPS})^2}{N}\right]}, \qquad (9)$$

where RMSE is the root-mean-square error between GPS observations and model results, N is the number of stations, x_i^{GPS} and x_i are the GPS observations and model results at the particular station i, respectively.

Initially, we used the horizontal displacements of GPS data only to constrain the viscosities of the middle-lower crust and upper mantle in the Songpan-Ganzi Block. The test model indicates that when the viscosities for the middle-lower crust and upper mantle in the Songpan-Ganzi Block are 5.62×10^{18} Pa·s and 5.89×10^{20} Pa·s, and the RMSE is the minimum. However, there are still some discrepancies in the near-field stations if only horizontal displacements are considered (Hu et al., 2021).

Thus, we then constrain the viscosities of the middle-lower crust and upper mantle in the Songpan-Ganzi Block using both the horizontal and vertical displacements of GPS data. Figure 5 shows the data misfit as a function of viscosities for the middle-lower crust and upper mantle in the Songpan-Ganzi Block. The results show that the optimal viscosities for the middle-lower crust and upper mantle in the Songpan-Ganzi Block are 6.61×10^{18} Pa·s and 1.12×10^{20} Pa·s, respectively.

The results show that the optimal viscosities for the middle-lower crust and upper mantle in the Songpan-Ganzi Block did not change much, and were within the same order of magnitude, between considering only horizontal displacements and considering both horizontal and vertical displacements. This consistency may be attributed to the relatively small magnitude and higher uncertainty associated with vertical displacements. The result is also consistent with previous studies (Hu et al., 2021; Zhang et al., 2021).

Figure 6 shows the comparison between the first 9-year surface displacements after the Wenchuan earthquake observed by GPS and that predicted in the model using the optimal viscosities (6.61×10^{18} Pa·s and 1.12×10^{20} Pa·s) of the middle-lower crust and upper mantle in the Songpan-Ganzi Block. The results show that the model can explain the observed post-seismic deformation well (both horizontal and vertical displacements). The results show both a continuous compression of the Songpan-Ganzi Block toward the South China Block overall, and an uplift of the Songpan-Ganzi Block.

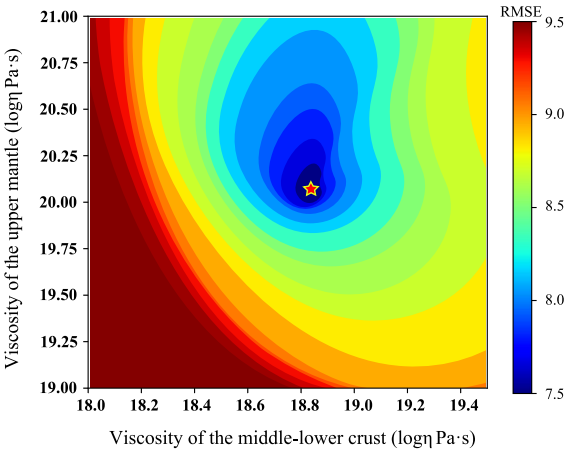

Figure 5
Data misfit map as function of viscosities of the Songpan-Ganzi Block. The red star represents the optimal fitting point

3.3. *Coulomb Stress Changes Caused by Wenchuan and Lushan Earthquakes*

The 2008 M_w7.9 Wenchuan earthquake and 2013 M_w6.6 Lushan earthquake occurred on the LMSF, which has attracted considerable attention (Guo et al., 2020; Liang et al., 2018; Liu et al., 2018; Parsons et al., 2008; Toda et al., 2008; Xu et al., 2013, 2020; Zhang et al., 2010). These two earthquakes did not entirely rupture the LMSF and there are two distinct seismic gaps on the LMSF (Dayi seismic gap and

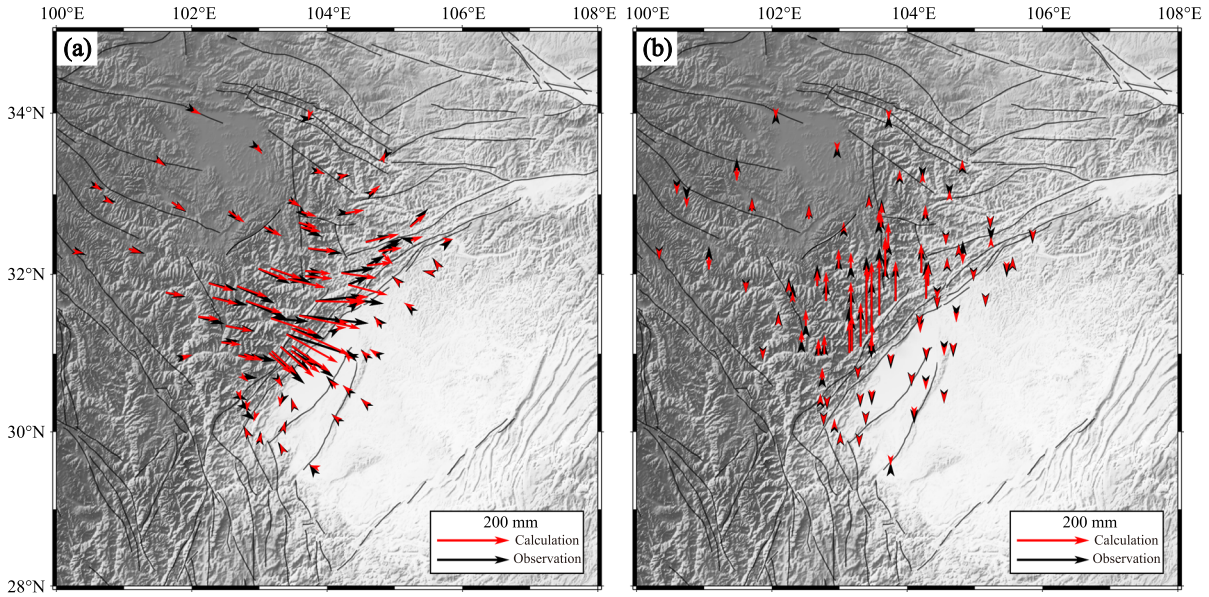

Figure 6
Comparison of post-seismic surface displacements 9 years after the Wenchuan earthquake between model results and GPS observations. **a** Comparison of post-seismic horizontal displacements. **b** Comparison of post-seismic vertical displacements. The red and black arrows show the model results and GPS observations (Wang et al., 2021), respectively

Tianquan-Kangding seismic gap) (Liang et al., 2018; Liu et al., 2020). To analyze the effects of the Wenchuan and Lushan earthquakes on these seismic gaps and other regions, we calculate the co-seismic and post-seismic Coulomb stress changes caused by the Wenchuan and Lushan earthquakes. Coulomb stress changes (ΔCFS) is defined as (King et al., 1994):

$$\Delta \mathrm{CFS} = \Delta\tau + \mu' \Delta\sigma_n, \tag{10}$$

where $\Delta\tau$ is the shear stress on the fault plane, $\Delta\sigma_n$ is the normal stress (tensile stress is positive) on the fault plane, and μ' is the effective friction coefficient ($\mu' = 0.4$ in this study). $\Delta CFS > 0$ indicates that the fault plane tends to move toward the failure and the seismic hazard increases, while $\Delta CFS < 0$ indicates that the fault plane tends to move away from the failure and the seismic hazard decreases (King et al., 1994; Stein, 1999).

Figure 7 illustrates the co-seismic Coulomb stress changes caused by the Wenchuan earthquake in four slip models (Fig. 3), which are projected to the plane (strike, 205°; dip, 33°; rake, 142°) of the Yingxiu-Beichuan fault (main seismogenic fault of the Wenchuan earthquake) (Shen et al., 2009; Zhou et al., 2006). The distribution of Coulomb stress changes exhibits differences among the different models, but also shows a certain degree of consistency. We further compared the correspondence between co-seismic Coulomb stress changes in different models and aftershocks of the Wenchuan earthquake. The spatial distribution of positive Coulomb stress changes calculated by the model proposed by Fielding et al. (2013) corresponds well with the aftershocks (Fig. 7d). These findings suggest that the model proposed by Fielding et al. (2013) provides a better explanation of the influence of co-seismic Coulomb stress changes on aftershocks. Therefore, it is reasonable for us to use the model of Fielding et al. (2013) to analyze Coulomb stress changes.

Figure 8a illustrates that the Wenchuan earthquake resulted in significant stress adjustments in the surrounding area, especially in the southern and northern LMSF (+ 0.005 ∼ + 1.175 MPa).

We also calculate the post-seismic Coulomb stress changes caused by the Wenchuan earthquake. The results (Fig. 8b), just before the 2013 M_w6.6 Lushan

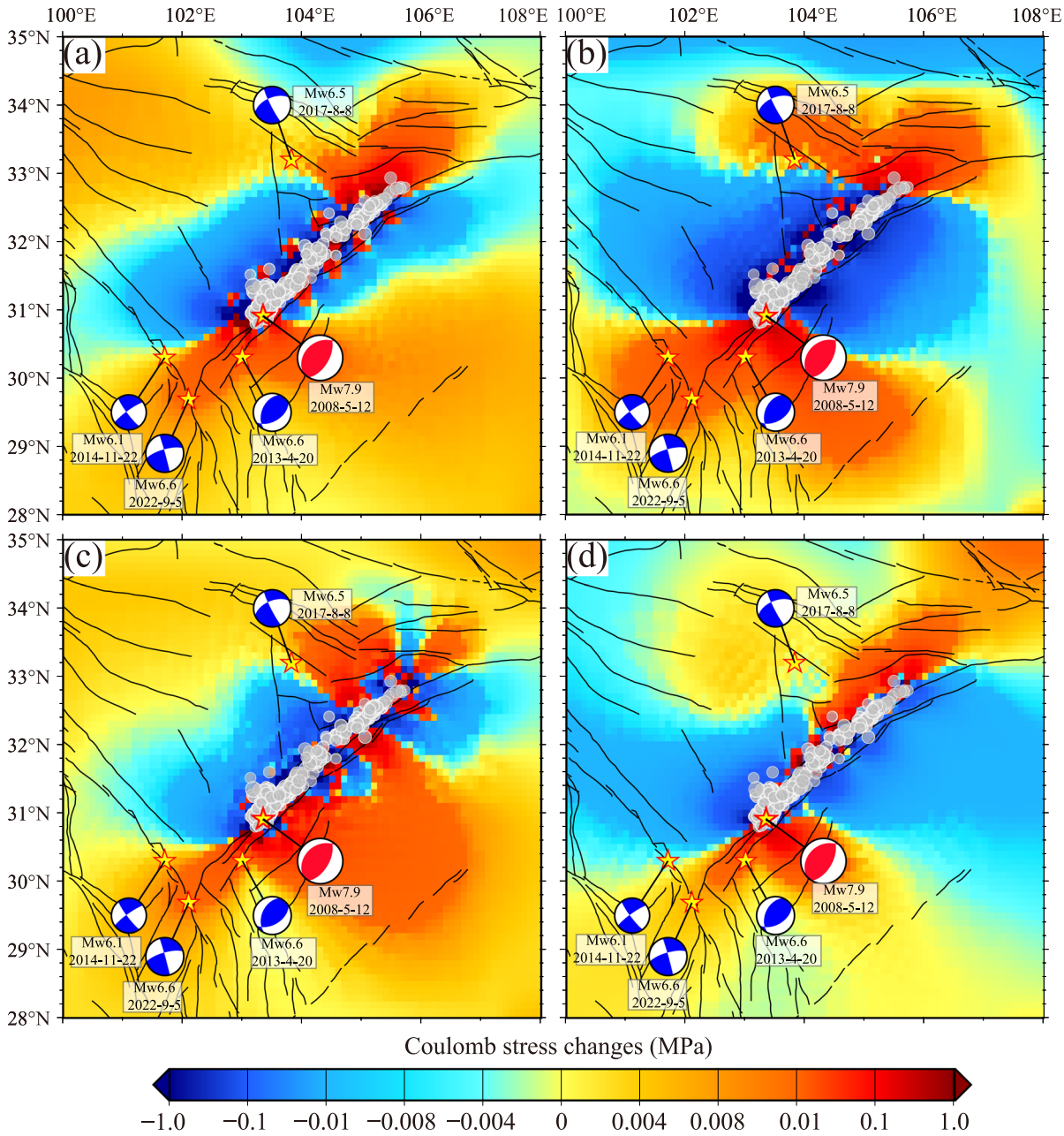

Figure 7
Co-seismic Coulomb stress changes caused by the Wenchuan earthquake calculated from different co-seismic slip models. **a**–**d** Results from the models of Ji (2008), Wang et al. (2008), Wang et al. (2011), and Fielding et al. (2013), respectively. The gray circles show the aftershocks of the Wenchuan earthquake

earthquake, show nearly the same spatial pattern with co-seismic Coulomb stress changes caused by the Wenchuan earthquake (Fig. 8a). The subsequent 2013 M_w6.6 Lushan earthquake occurred on the southern LMSF, where the Coulomb stress changes caused by the Wenchuan earthquake is nearly + 0.068 ∼ + 0.144 MPa (co-seismic Coulomb stress changes, + 0.063 ∼ + 0.132 MPa; post-seismic

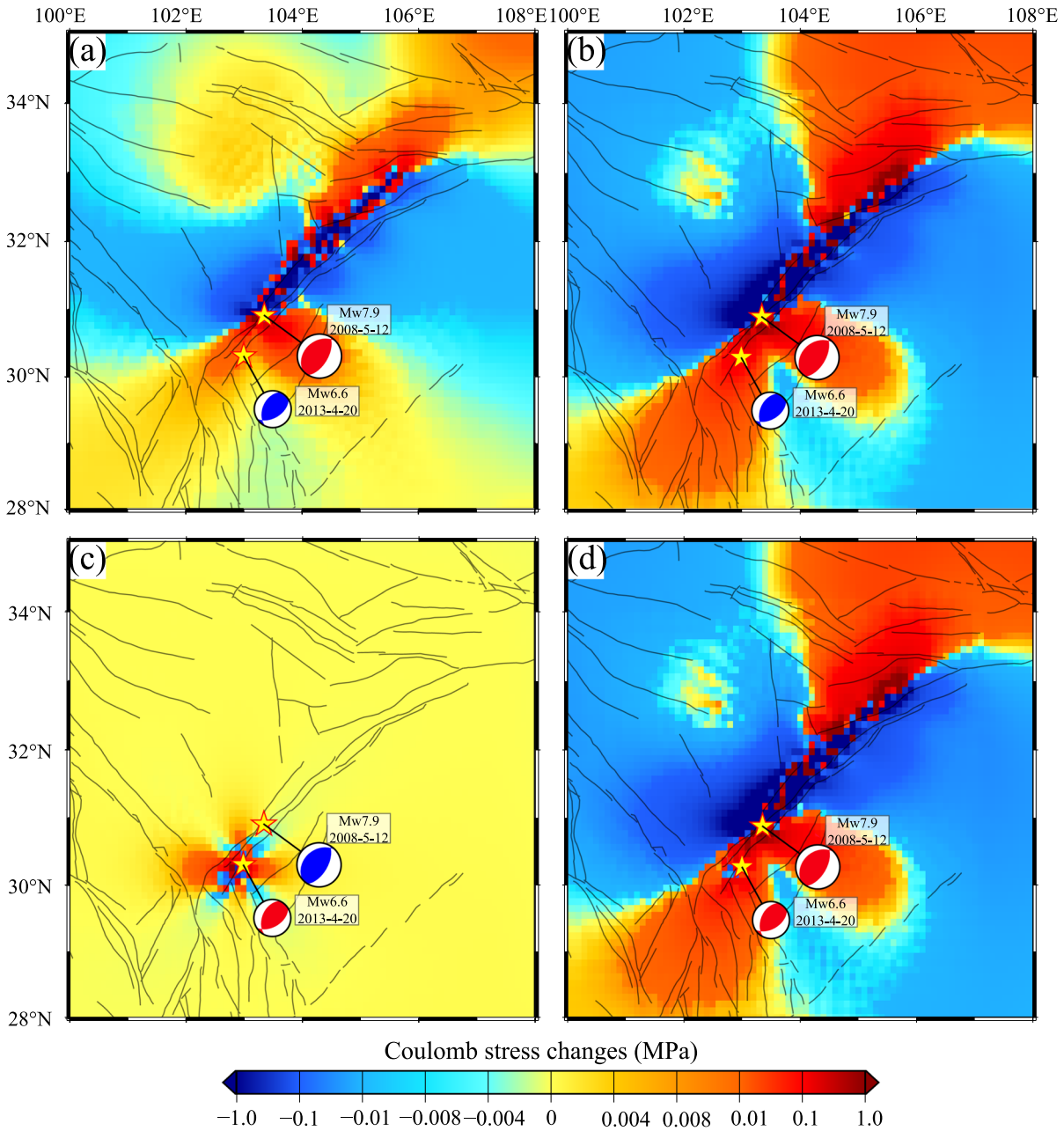

Figure 8

Coulomb stress changes caused by the Wenchuan and Lushan earthquakes. **a** Co-seismic Coulomb stress of the Wenchuan earthquake calculated using the model of Fielding et al. (2013). **b** Coulomb stress (co-seismic and post-seismic) generated by the Wenchuan earthquake prior to the Lushan earthquake. **c** Co-seismic Coulomb stress changes of Lushan earthquake. **d** Coulomb stress changes (co-seismic and post-seismic) caused by the Wenchuan and Lushan earthquakes (10 years after the Lushan earthquake)

Coulomb stress changes, + 0.005 ∼ + 0.012 MPa). It appears that the value has surpassed the triggering threshold of 0.01 MPa (Freed, 2005; King et al., 1994), implying a high probability that the Wenchuan earthquake triggered the Lushan earthquake.

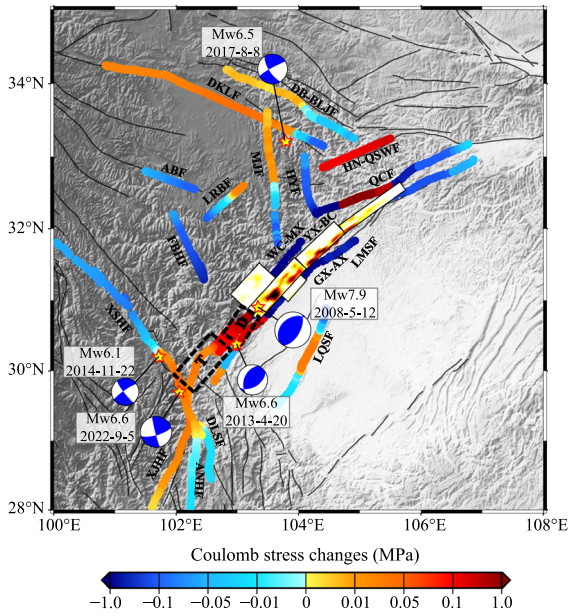

Figure 9
Cumulative Coulomb stress changes caused by the Wenchuan and Lushan earthquakes on major faults in the eastern Tibetan Plateau. Labels are explained in Fig. 1

The results of co-seismic Coulomb stress changes caused by the Lushan earthquake are relatively small, and its impact was limited (Fig. 8c).

We found that stress states in the Dayi and Tianquan-Kangding seismic gaps are significantly influenced by the Wenchuan and Lushan earthquakes (Fig. 8d). Though there are negative co-seismic Coulomb stress changes caused by the Lushan earthquake observed in certain parts of these two seismic gaps, the value is relatively small (Fig. 8c). Coulomb stress changes caused by the Wenchuan and Lushan earthquakes are + 0.216 ∼ + 2.607 MPa and + 0.021 ∼ + 0.211 MPa in Dayi seismic gap and Tianquan-Kangding seismic gap, respectively (Fig. 8d).

Table 2

Parameters of main active faults in the study area

Fault name	Strike/(°)	Dip/(°)	Rake/(°)
XSHF	142–160	90	0–45
FBHF	145	80	10
MJF	180	45–56	45
DKLF	100–145	89	0
HYF	150	75	45
ABF	295	60–80	90
DB-BLJF	290	68–85	45
LQSF	210	50	90
QCF	70	75	170
HN-QSWF	69	70	45
LRBF	205–229	60	135
DLSF	150–159	75–90	0–45
XJHF	200	80–90	0–30
ANHF	159	90	45
WC-MX	220–225	23–50	100–104
GX-AX	200–207	44	94
YX-BC	205	33	142

To further investigate the effects of the Wenchuan and Lushan earthquakes on the regional fault system and analyze regional seismic hazards, we calculate the cumulative Coulomb stress changes (including both co-seismic and post-seismic Coulomb stress changes caused by the Wenchuan and Lushan earthquakes) projected onto each fault plane on the regional fault system (Fig. 9). Detailed fault parameters are shown in Table 2 (Clarence et al., 1991; He & Chéry, 2008; He et al., 2008; Zhou et al., 1999), with median value selected for the floating parameters. Our results demonstrate that Coulomb stress changes caused by the Wenchuan and Lushan earthquakes have significant effects on regional fault system (Fig. 9). In general, Coulomb stress changes increase predominantly in the southern LMSF, southern XSHF (encompassing the Kangding-Shimian segment and Daofu-Kangding segment), XJHF, central LQSF, western QCF, HN-QSWF, western DB-BLJF, northern MJF, DKLF, and northern LRBF (Fig. 9). Across most of above fault segments, Coulomb stress changes exceed 0.01 MPa, indicating a heightened risk of seismic hazards in these regions. Coulomb stress changes decrease in the northern XSHF, northern LMSF, ANHF, DLSF, southern MJF, southern LRBF, FBHF, ABF, eastern DB-BLJF, and HYF (Fig. 9).

We note that several earthquakes in the vicinity (2014 M_w6.1 Kangding earthquake, 2017 M_w6.5 Jiuzhaigou earthquake, and 2022 M_w6.6 Luding earthquake) occurred in regions with positive Coulomb stress changes (Fig. 9) caused by the Wenchuan and Lushan earthquakes. These findings provide evidence of triggering between these earthquakes.

While it is widely accepted that large earthquakes can trigger subsequent earthquakes in the surrounding area through positive Coulomb stress changes (King

et al., 1994; Parsons et al., 2008; Stein, 1999), it should be noted that these changes represent second-order perturbations of stress on nearby faults (King et al., 1994; Tormann et al., 2015). Many studies have also found that some subsequent earthquakes occur in areas with negative Coulomb stress changes caused by preceding earthquakes (Gkarlaouni et al., 2008; Luo & Liu, 2018). In fact, Coulomb stress changes triggered by earthquakes on surrounding faults is a relatively small perturbation (Luo & Liu, 2018; Sun et al., 2020), compared to the background stress already accumulated on those faults. The background stress plays a critical role in determining whether an earthquake will occur. Thus, to better understand regional seismic hazards, it is crucial to conduct a comprehensive analysis of total stress evolution on faults.

3.4. *Spatial Distribution of b-Values in the Eastern Tibetan Plateau*

The magnitude–frequency relationship (also called the G–R relationship) is one of the most important statistical relationships for describing seismic activity (Gutenberg & Richter, 1944). The relationship between magnitude and frequency can be expressed as follows:

$$LgN = a - bM, \tag{11}$$

where M is the magnitude of the earthquake ($M \geq M_c$), M_c is the minimum complete magnitude, and N is the cumulative frequency of earthquakes. The parameter a is the constant reflecting the regional seismicity, and the parameter b is the relative proportion of large and small earthquakes in a region.

The b-value has attracted considerable attention (Kun et al., 2013; Liu & Pei, 2017; Main et al., 1992; Scholz, 2015; Schorlemmer et al., 2005). Rock fracture experiments (Main et al., 1992; Scholz, 1968), numerical simulation (Gao et al., 2020), and statistical results of regional seismicity (Kun et al., 2013; Schorlemmer et al., 2005; Zhang & Zhou, 2016) all indicate that the b-value has a clear physical meaning. A lower b-value indicates a higher stress level in a region, while a higher b-value indicates a lower stress level in a region. Thus, we then calculate the regional b-value to further estimate the stress level in the eastern Tibetan Plateau before the 2008 M_w7.9 Wenchuan earthquake.

The seismic catalog from 1970 to 2008 used in this study is provided by the China Earthquake Network Center. Figure 10 shows the statistical results of seismic activity over time based on the regional catalog. The results show that the cumulative and annual frequency of earthquakes is roughly bounded by the year 2000 (red dashed line in Fig. 10). Specifically, the cumulative rate and annual frequency of earthquakes prior to 2000 is notably lower than that observed after 2000. We note that the Regional Telemetered Digital Seismograph Network of China underwent its second update around the year 2000 (Liu et al., 2003), resulting in a significant improvement in its monitoring capabilities. It is generally considered that the seismic catalog after the

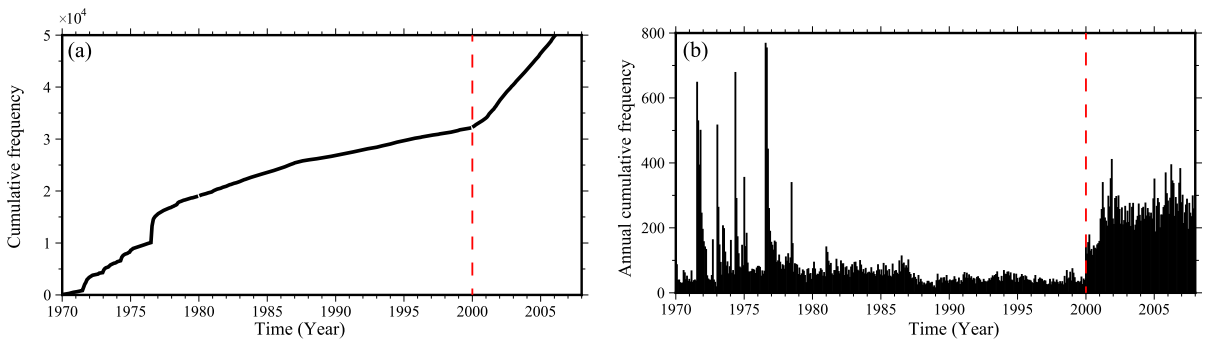

Figure 10
Statistics of instrumental earthquakes in the eastern Tibetan Plateau. **a** and **b** Cumulative and annual frequency of earthquakes from 1970 to 2008, respectively

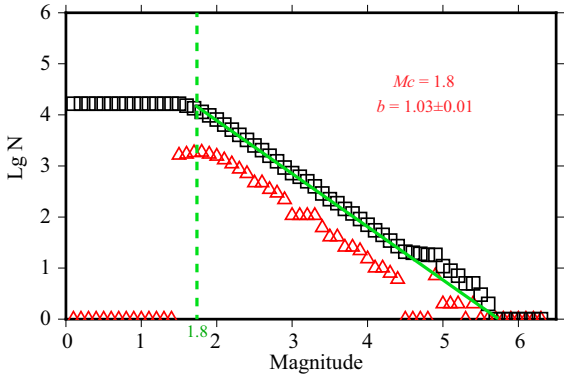

Figure 11
Earthquake magnitude–frequency distribution. The non-cumulative and cumulative magnitude–frequency distributions are represented by the red triangles and black squares, respectively

year 2000 is more complete. Therefore, we selected the catalog from 2000 to 2008 for our calculations.

Figure 11 shows the magnitude–frequency distribution based on the seismic catalog from 2000 to 2008. We use the maximum curvature method (Wiemer & Wyss, 2000) to calculate the minimum completed magnitude M_c and the maximum likelihood method (Aki, 1965) to calculate the regional b-values. The results show that $M_c = 1.8$ and $b = 1.03 \pm 0.01$. The b-value is also approximately similar to the global average of 1.0 (El-Isa & Eaton, 2014).

To further analyze the spatial distribution of regional b-values, the study area is subdivided into $0.1° \times 0.1°$ grids. We calculate the M_c and b-value at each grid node with an initial statistical radius $R = 20$ km. We prescribed the number of earthquakes $N \geq 50$ within the statistical radius and the magnitude span $M_{span} \geq 2.5$ (Kutliroff, 2017). If the prescribed number of earthquakes and magnitude span were not satisfied, we increase the statistical radius by 10 km. However, we also impose a condition that the statistical radius should not exceed 60 km. If seismic data within a grid node do not satisfy the preset conditions, M_c and b-values in this grid node were not calculated.

Figure 12a shows the spatial distribution of M_c. The results show that M_c across the eastern Tibetan Plateau generally ranges from 1.2 to 2.0. Figure 12b shows the spatial distribution of the b-values, with notably lower values found near the faults, including the middle segment of LMSF, XSHF, XJHF, FBHF, HN-QSWF, and DKLF. It is noteworthy that the study area has recently experienced several large earthquakes, including the 2008 M_w7.9 Wenchuan,

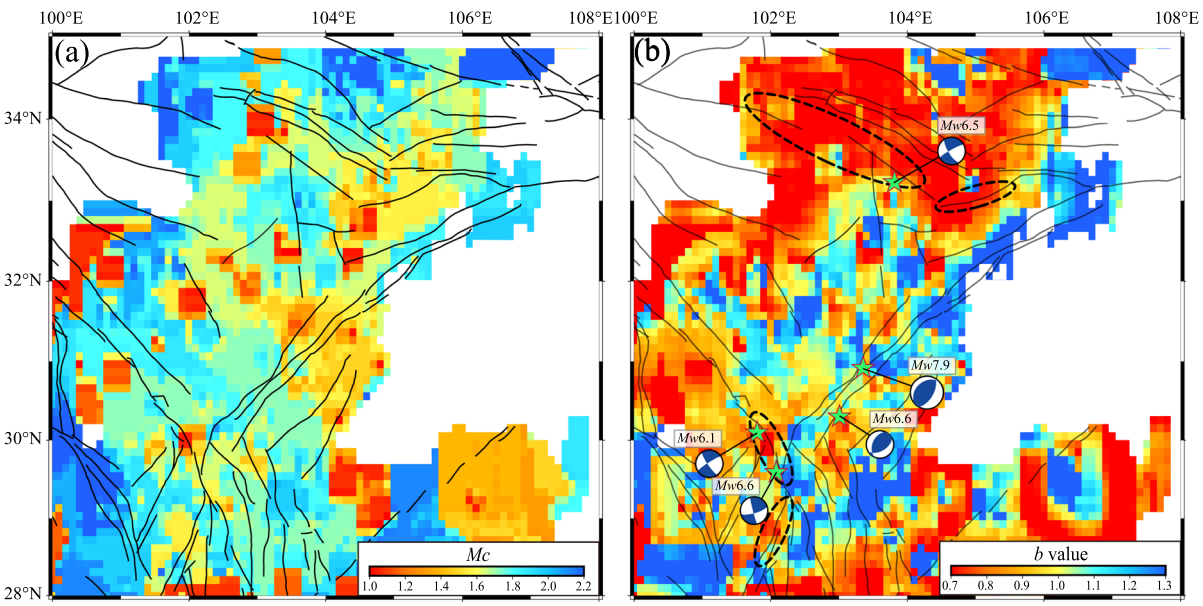

Figure 12
Spatial distribution of M_c (**a**) and b-values (**b**) in the eastern Tibetan Plateau before the Wenchuan earthquake

2013 M_w6.6 Lushan, 2014 M_w6.1 Kangding, 2017 M_w6.5 Jiuzhaigou, and 2022 M_w6.6 Luding earthquakes, all of which occurred in regions with low *b*-values. Since the *b* value is negatively correlated with stress (Kun et al., 2013; Main et al., 1992; Nuannin et al., 2012; Scholz, 1968, 2015; Schorlemmer et al., 2004, 2005), high stress has already accumulated in these regions prior to these earthquakes. Thus, the *b*-value may be an important indicator of regional seismic hazards.

4. Discussion

In this study, we set up a 3D viscoelastic finite element model in the eastern Tibetan Plateau, and calculate Coulomb stress changes caused by 2008 M_w7.9 Wenchuan and 2013 M_w6.6 Lushan earthquakes. The computation of Coulomb stress changes is significantly influenced by the slip model of large earthquakes and viscosities of the middle-lower crust and upper mantle. Thus, we analyze four slip models of the Wenchuan earthquake and choose the viscoelastic model that produced the closest match to the GPS data. Based on the chosen slip model of the Wenchuan earthquake, we also invert the viscosities of the middle-lower crust and upper mantle for the Songpan-Ganzi Block.

The results show that Coulomb stress changes caused by the Wenchuan earthquake near the epicenter of 2013 M_w6.6 Lushan earthquake is positive ($+0.063 \sim +0.132$ MPa and $+0.005 \sim +0.012$ MPa for co-seismic and post-seismic Coulomb stress changes, respectively) (Fig. 8b), and the total value exceeds the threshold of 0.01 MPa (Freed, 2005; King et al., 1994). This suggests that the Wenchuan earthquake indeed triggered the occurrence of the Lushan earthquake, which is generally consistent with previous studies (Guo et al., 2020; Nalbant & McCloskey, 2011; Parsons et al., 2008; Toda et al., 2008).

Coulomb stress evolutions caused by the Wenchuan and Lushan earthquakes have a significant impact on regional fault system (Fig. 9). Overall, Coulomb stress changes increase mainly in the southern LMSF, southern XSHF (encompassing the Kangding-Shimian segment and Daofu-Kangding segment), XJHF, central LQSF, western QCF, HNQSWF, western DB-BLJF, northern MJF, DKLF, and northern LRBF. We found that recent earthquakes (2014 M_w6.1 Kangding earthquake, 2017 M_w6.5 Jiuzhaigou earthquake, and 2022 M_w6.6 Luding earthquake) occurred in regions where Coulomb stress changes caused by the Wenchuan and Lushan earthquakes are positive. However, there are still many regions with highly positive Coulomb stress changes that have not experienced major earthquakes yet (Fig. 9), and these regions are deemed high potential for seismic hazards in the future. We also noticed that Coulomb stress changes between the Dayi and Tianquan-Kangding seismic gaps are far greater than 0.01 MPa (Fig. 9).

Compared with background stress already accumulated on faults, Coulomb stress changes caused by earthquakes is a relatively small perturbation (Luo & Liu, 2018; Sun et al., 2020). However, when the background stress (stress already accumulated on faults) is relatively high and in the critical state of failure on faults, the increased Coulomb stress changes may trigger the subsequent earthquakes.

Previous studies have indicated that seismic *b*-values decrease linearly with increasing stress (Kun et al., 2013; Main et al., 1992; Nuannin et al., 2012; Scholz, 1968; Schorlemmer et al., 2004). To better understand the background stress state in the eastern Tibetan Plateau, we then analyze the spatial distribution of *b*-values using the regional catalog from 2000 to 2008. The findings suggest that numerous earthquakes, including the 2008 M_w7.9 Wenchuan earthquake, 2013 M_w6.6 Lushan earthquake, 2014 M_w6.1 Kangding earthquake, 2017 M_w6.5 Jiuzhaigou earthquake, and 2022 M_w6.6 Luding earthquake, occurred in areas with low *b*-values (Fig. 12), which is consistent with other studies (Zhang & Zhou, 2016; Zhao et al., 2019). This implies that these regions already have a high background stress level, increases of Coulomb stress changes (Fig. 9) could trigger subsequent earthquakes. Therefore, an assessment of seismic hazards utilizing both Coulomb stress changes and seismic *b*-values proves a more comprehensive approach for regional seismic analysis.

By integrating the Coulomb stress changes resulting from earthquakes and the *b*-value

distribution, we identified four fault segments (southern XSHF, northern XJHF, DKLF, and HN-QSWF) with both low *b*-values and positive Coulomb stress changes (black dashed circles in Fig. 12b). Among these areas, only two have witnessed subsequent large earthquakes, namely the 2014 M_w6.1 Kangding earthquake, 2017 M_w6.5 Jiuzhaigou earthquake, and 2022 M_w6.6 Luding earthquake. In contrast, no major earthquakes have occurred in other regions yet, indicating an increased potential for seismic hazards in the future.

Our finite element model used in the calculations is relatively simplified and did not take into account historical earthquakes, the dynamic propagation of seismic waves, and tectonic loading. Therefore, future research could incorporate these factors to provide more comprehensive references for regional seismic hazard analysis.

5. Conclusion

In this study, we constructed a 3D viscoelastic finite element model to calculate Coulomb stress changes caused by the Wenchuan and Lushan earthquakes. We also calculated the spatial distribution of regional *b*-values. We then combined the stress transfer between earthquakes with the spatial distribution of *b*-values to assess seismic hazards in the area. Our main conclusions from this study are as follows:

1. Constrained by 9-year post-seismic deformation due to the 2008 M_w7.9 Wenchuan earthquake, we estimated the optimal viscosities for the middle-lower crust and upper mantle in the Songpan-Ganzi Block as 6.61×10^{18} Pa·s and 1.12×10^{20} Pa·s, respectively.
2. Regional earthquakes (including the 2008 M_w7.9 Wenchuan earthquake, 2013 M_w6.6 Lushan earthquake, 2014 M_w6.1 Kangding earthquake, 2017 M_w6.5 Jiuzhaigou earthquake, and 2022 M_w6.6 Luding earthquake) occurred in regions with low *b*-values. Meanwhile, subsequent earthquakes occurred in regions where Coulomb stress changes caused by the Wenchuan and Lushan earthquakes were positive. This suggests that regions with both low *b*-values and positive Coulomb stress changes may pose higher seismic hazards.
3. After the Wenchuan and Lushan earthquakes, there are four regions (southern Xianshuihe fault, Dongkunlun fault, northern Xiaojinhe fault, and Hanan-Qingshanwan fault) with both highly positive Coulomb stress changes and low *b*-values, which may indicate high-stress accumulation and high seismic hazard in the future.
4. Coulomb stress changes caused by the Wenchuan and Lushan earthquakes increased significantly in the Dayi seismic gap (+0.216 ∼ +2.607 MP), and Tianquan-Kangding seismic gap (+0.021 ∼ +0.211 MPa), while the result of high *b*-values for both seismic gap indicates relatively low accumulation of background stress. However, with continued tectonic loading, seismic hazards on both seismic gaps should cause our attention.

Acknowledgements

The GPS data used in this study can be found at https://doi.org/10.7910/DVN/V5LIHG. The seismic data used in this study are available from the China Earthquake Data Center (http://data.earthquake.cn/index.html). We appreciate Chung-Han Chan and two anonymous reviewers for constructive suggestions and comments.

Author contributions SY (First Author): conceptualization, methodology, software, formal analysis, supervision, writing—original draft, writing—review and editing; GW: methodology, software, formal analysis, data curation, writing—original draft, writing—review and editing; WF: writing—review and editing; JW (Corresponding Author): writing—review and editing, supervision

Funding

This research is supported by the National Natural Science Foundation of China (42104094), Natural Science Foundation of Fujian Province (2022J05039), and Open Foundation of the United Laboratory of Numerical Earthquake Forecasting (2021LNEF03).

Declarations

Conflict of interest The authors declare no competing interests.

Publisher's Note Springer Nature remains neutral with regard to jurisdictional claims in published maps and institutional affiliations.

References

Aki, K. (1965). Maximum likelihood estimate of b in the formula logN=a-bM and its confidence limits. *Bulletin of the Earthquake Research Institute, University of Tokyo, 43*, 237–239.

Bao, X., Song, X., Eaton, D. W., Xu, Y., & Chen, H. (2020). Episodic lithospheric deformation in eastern Tibet inferred from seismic anisotropy. *Geophysical Research Letters*. https://doi.org/10.1029/2019gl085721

Chai, T., & Draxler, R. R. (2014). Root mean square error (RMSE) or mean absolute error (MAE). *Geoscientific Model Development Discussions, 7*(1), 1525–1534. https://doi.org/10.5194/gmd-7-1247-2014

Chen, Y., Yang, Z., Zhang, Y., & Liu, C. (2013). From the Wenchuan Earthquake to the Lushan Earthquake. *Science China Earth Sciences, 43*(6), 1064–1072. https://doi.org/10.1360/zd-2013-43-6-1064

Clarence, R. A., Luo, Z., Qian, H., Wen, X., Zhou, H., & Huang, W. (1991). Field study of a highly active fault zone: The Xianshuihe fault of southwestern China. *Geological Society of America Bulletin, 103*(9), 1178–1199.

Deng, Q., Chen, S., & Zhao, X. (1994). Tectonics, seismicity and dynamics of Longmenshan mountains and its adjacent regions. *Seismology and Geology*, *16*(4), 389–403.

Deng, Q., Zhang, P., Ran, Y., Yang, X., Min, W., & Chu, Q. (2003). Basic characteristics of active tectonics of China. *Science in China Series D: Earth Sciences, 46*(4), 356–372. https://doi.org/10.1360/03yd9032

Diao, F., Wang, R., Wang, Y., Xiong, X., & Walter, T. R. (2018). Fault behavior and lower crustal rheology inferred from the first seven years of postseismic GPS data after the 2008 Wenchuan earthquake. *Earth and Planetary Science Letters, 495*, 202–212. https://doi.org/10.1016/j.epsl.2018.05.020

Dong, L., Zhang, L., Liu, H., Du, K., & Liu, X. (2022). Acoustic Emission b Value Characteristics of Granite under True Triaxial Stress. *Mathematics, 10*(3), 451. https://doi.org/10.3390/math10030451

Dong, S., Han, Z., & An, Y. (2017). Paleoseismological events in the "seismic gap" between the 2008 Wenchuan and the 2013 Lushan earthquakes and implications for future seismic potential. *Journal of Asian Earth Sciences, 135*, 1–15. https://doi.org/10.1016/j.jseaes.2016.12.016

El-Isa, Z. H., & Eaton, D. W. (2014). Spatiotemporal variations in the b-value of earthquake magnitude–frequency distributions: Classification and causes. *Tectonophysics, 615*, 1–11. https://doi.org/10.1016/j.tecto.2013.12.001

Feng, S., Zhang, P., Liu, B., Wang, M., Zhu, S., Ran, Y., Wang, W., Zhang, Z., Zheng, W., Zheng, D., Zhang, H., & Tian, X. (2016). Deep crustal deformation of the Longmen Shan, eastern margin of the Tibetan Plateau, from seismic reflection and Finite Element modeling. *Journal of Geophysical Research: Solid Earth, 121*(2), 767–787. https://doi.org/10.1002/2015JB012352

Fielding, E. J., Sladen, A., Li, Z., Avouac, J., Bürgmann, R., & Ryder, I. (2013). Kinematic fault slip evolution source models of the 2008 M7.9 Wenchuan earthquake in China from SAR interferometry, GPS and teleseismic analysis and implications for Longmen Shan tectonics. *Geophysical Journal International, 194*(2), 1138–1166. https://doi.org/10.1093/gjilggt155

Freed, A. M. (2005). Earthquake triggering by static, dynamic, and postseismic stress transfer. *Annual Review of Earth and Planetary Sciences, 33*(1), 335–367.

Gao, J., Li, Y., Wang, Z., Zhang, Y., Jia, L., & Li, D. (2022). Crustal velocity structure of the southeastern Tibetan plateau and its geological implications for the Yunnan Yangbi Ms 6.4 earthquake. *Chinese Journal of Geophysics, 65*(2), 604–619. https://doi.org/10.6038/cjg2022P0354

Gao, Y., Luo, G., & Sun, Y. (2020). Seismicity, fault slip rates, and fault interactions in a fault system. *Journal of Geophysical Research: Solid Earth, 125*(2), e2019JB017379. https://doi.org/10.1029/2019JB017379

Gkarlaouni, C., Papadimitriou, E. E., Karakostas, V. G., Wen, X., Jin, X., Kilias, A., Pan, H., & Yang, J. (2008). Implication of fault interaction to seismic hazard assessment in Sichuan-Yunnan provinces of southeastern China. *Acta Seismologica Sinica, 21*(2), 181–201. https://doi.org/10.1007/s11589-008-0009-7

Gong, W., Sun, Y., Qiu, X., Wang, G., Li, M., & Ruan, Y. (2023). Coulomb stress evolution and seismic hazards along major faults in the northeastern margin of the Tibetan Plateau. *China Earthquake Engineering Journal, 45*(3), 585–597. https://doi.org/10.20000/j.1000-0844.20221226001

Guo, R., Zheng, Y., & Xu, J. (2020). Stress modulation of the seismic gap between the 2008 Ms8.0 Wenchuan earthquake and the 2013 Ms7.0 Lushan earthquake and implications for seismic hazard. *Geophysical Journal International, 221*(3), 2113–2125. https://doi.org/10.1093/gji/ggaa143

Gutenberg, B., & Richter, C. F. (1944). Frequency of earthquakes in California. *Bulletin of the Seismological Society of America, 34*(4), 185–188. https://doi.org/10.1785/BSSA0340040185

He, H., Yasutaka, I., He, Y., Masami, T., Chen, J., Chan, C., Zhenghao, t, Tomoo, E., & Shinsuke, O. (2008). The Emerging Daliang Shan Fracture Zone-Cutting and Straightening the Middle Section of the Xiangshuihe-Xiaojiang Fracture System. *Science China Earth Sciences, 38*(5), 564–574. https://doi.org/10.1360/zd2008-38-5-564

He, J., & Chéry, J. (2008). Slip rates of the Altyn Tagh, Kunlun and Karakorum faults (Tibet) from 3D mechanical modeling. *Earth and Planetary Science Letters, 274*(1–2), 50–58. https://doi.org/10.1016/j.epsl.2008.06.049

Hu, Y., Bürgmann, R., Uchida, N., Banerjee, P., & Freymueller, J. T. (2016). Stress-driven relaxation of heterogeneous upper

mantle and time-dependent afterslip following the 2011 Tohoku earthquake. *Journal of Geophysical Research: Solid Earth, 121*(1), 385–411. https://doi.org/10.1002/2015jb012508

Hu, Z., Hu, Y., & Bodunde, S. (2021). Viscoelastic relaxation of the upper mantle and afterslip following the 2014 Mw8.1 Iquique earthquake. *Earthquake Research Advances, 1*(100002), 1–7. https://doi.org/10.1016/j.eqrea.2021.100002

Ji, C. (2008). Preliminary result of the May 12, 2008 Mw7.97 Sichuan earthquake. Retrieved October 10, 2023, from https://ji.faculty.geol.ucsb.edu/big_earthquakes/2008/05/12/ShiChuan.html

King, G. C. P., Stein, R. S., & Lin, J. (1994). Static stress changes and the triggering of earthquakes. *Bulletin of the Seismological Society of America, 84*(3), 935–953. https://doi.org/10.1785/bssa0840030935

Kun, F., Varga, I., Lennartz-Sassinek, S., & Main, I. G. (2013). Approach to failure in porous granular materials under compression. *Physical Review E, 88*(6), 062207. https://doi.org/10.1103/PhysRevE.88.062207

Kutliroff, J. R. (2017). Estimating the proportions of large to small earthquakes in seismic regions with a short span of earthquake magnitudes. The University of Memphis.

Li, B., Xie, F., Huang, J., Xu, X., Guo, Q., Zhang, G., Xu, J., Wang, J., Jiang, D., & Wang, J. (2022). In situ stress state and seismic hazard in the Dayi seismic gap of the Longmenshan thrust belt. *Science China Earth Sciences, 65*(7), 1388–1398. https://doi.org/10.1007/s11430-021-9915-4

Li, Y., Shan, X., Gao, Z., & Huang, X. (2023). Interseismic Coupling, Asperity Distribution, and Earthquake Potential on Major Faults in Southeastern Tibet. *Geophysical Research Letters*. https://doi.org/10.1029/2022gl101209

Li, Y., Zhang, G., Shan, X., Liu, Y., Wu, Y., Liang, H., Qu, C., & Song, X. (2018). GPS-derived fault coupling of the Longmenshan fault associated with the 2008 Mw Wenchuan 7.9 earthquake and its tectonic implications. *Remote Sensing, 10*(5), 753. https://doi.org/10.3390/rs10050753

Liang, C., Huang, Y., Wang, C., Liu, Z., Yang, Y., Wu, J., & He, F. (2018). Progress in the studies of the seismic gap between the 2008 Wenchuan and 2013 Lushan earthquakes. *Chinese Journal of Geophysics, 61*(5), 1996–2010. https://doi.org/10.6038/cjg2018M0254

Liu, C., Zheng, Y., Ge, C., Xiong, X., & Xu, H. (2013). Dynamic rupture process of the 2013 Lushan County, Sichuan magnitude 7.0 earthquak. *Science China Earth Sciences, 43*(6), 1020–1026. https://doi.org/10.1360/zd-2013-43-6-1020

Liu, C., Zhu, B., & Shi, Y. (2020). Do the two seismic gaps in the Southwestern section of the Longmen Shan fault present the same seismic hazard? *Journal of Geophysical Research: Solid Earth, 125*(3), e2019JB018160. https://doi.org/10.1029/2019jn018160

Liu, R., Wu, Z., Yin, C., Chen, Y., & Zhuang, C. (2003). Development of China digital seismological observational systems. *Acta Seismologica Sinica, 16*(5), 568–573. https://doi.org/10.1007/BF02893477

Liu, Y., & Pei, S. (2017). Temporal and spatial variation of b-value before and after Wenchuan earthquake and its tectonic implication. *Chinese Journal of Geophysics, 60*(6), 2104–2112. https://doi.org/10.6038/cjg20170607

Liu, Z., Liang, C., Hua, Q., Li, Y., Yang, Y., He, F., & Fang, L. (2018). The seismic potential in the seismic gap between the Wenchuan and Lushan earthquakes revealed by the joint inversion of receiver functions and ambient noise data. *Tectonics, 37*(11), 4226–4238. https://doi.org/10.1029/2018TC005151

Luo, G., & Liu, M. (2018). Stressing rates and seismicity on the major faults in eastern Tibetan Plateau. *Journal of Geophysical Research: Solid Earth, 123*(12), 10968–10986. https://doi.org/10.1029/2018jb015532

Main, I. G., Meredith, P. G., & Sammonds, P. R. (1992). Temporal variations in seismic event rate and b-values from stress corrosion constitutive laws. *Tectonophysics, 211*(1–4), 233–246. https://doi.org/10.1016/0040-1951

Melosh, H., & Raefsky, A. (1981). A simple and efficient method for introducing faults into finite element computations. *Bulletin of the Seismological Society of America, 71*(5), 1391–1400. https://doi.org/10.1785/BSSA0710051391

Nalbant, S. S., & McCloskey, J. (2011). Stress evolution before and after the 2008 Wenchuan, China earthquake. *Earth and Planetary Science Letters, 307*(1–2), 222–232. https://doi.org/10.1016/j.epsl.2011.04.039

Nuannin, P., Kulhánek, O., & Persson, L. (2012). Variations of b-values preceding large earthquakes in the Andaman-Sumatra subduction zone. *Journal of Asian Earth Sciences, 61*, 237–242. https://doi.org/10.1016/j.jseaes.2012.10.013

Parsons, T., Ji, C., & Kirby, E. (2008). Stress changes from the 2008 Wenchuan earthquake and increased hazard in the Sichuan basin. *Nature, 454*(7203), 509–510. https://doi.org/10.1038/nature07177

Pei, S., Zhang, H., Su, J., & Cui, Z. (2014). Ductile gap between the Wenchuan and Lushan earthquakes revealed from the two-dimensional Pg seismic tomography. *Scientific Reports, 4*(1), 1–6. https://doi.org/10.1038/srep06489

Royden, L. H., Burchfiel, B. C., & Van der Hilst, R. D. (2008). The geological evolution of the Tibetan Plateau. *Science, 321*(5892), 1054–1058. https://doi.org/10.1126/science.1155371

Scholz, C. H. (1968). The frequency-magnitude relation of microfracturing in rock and its relation to earthquakes. *Bulletin of the Seismological Society of America, 58*(1), 399–415. https://doi.org/10.1785/BSSA0580010399

Scholz, C. H. (2015). On the stress dependence of the earthquake b value. *Geophysical Research Letters, 42*(5), 1399–1402. https://doi.org/10.1002/2014GL062863

Schorlemmer, D., Wiemer, S., & Wyss, M. (2005). Variations in earthquake-size distribution across different stress regimes. *Nature, 437*(7058), 539–542. https://doi.org/10.1038/nature04094

Schorlemmer, D., Wiemer, S., Wyss, M., & Jackson, D. D. (2004). Earthquake statistics at Parkfield: 2. Probabilistic forecasting and testing. *Journal of Geophysical Research: Solid Earth*. https://doi.org/10.1029/2004jb003235

Shao, Z., Wang, R., Wu, Y., & Zhang, L. (2011). Rapid afterslip and short-term viscoelastic relaxation following the 2008 Mw7.9 Wenchuan earthquake. *Earthquake Science, 24*(2), 163–175. https://doi.org/10.1007/s11589-010-0781

Shao, Z., Wang, W., Liu, Q., Pan, Z., Liu, X., Wang, P., Wei, W., Feng, W., & Yin, X. (2022). Perspectives on physical forecasting of earthquakes in the framework of active massif theory. *Chinese Science Bulletin, 67*(13), 1362–1377. https://doi.org/10.1360/TB-2021-0968

Shen, Z., Sun, J., Zhang, P., Wan, Y., Wang, M., Bürgmann, R., Zeng, Y., Gan, W., Liao, H., & Wang, Q. (2009). Slip maxima at fault junctions and rupturing of barriers during the 2008 Wenchuan earthquake. *Nature Geoscience, 2*(10), 718–724.

Shi, Y., & Cao, J. (2008). Effective viscosity of China continental lithosphere. *Earth Science Frontiers, 15*(3), 82–95.

Shi, Y., Sun, Y., Luo, G., Dong, P., & Zhang, H. (2018). Roadmap for earthquake numerical forecasting in China-Reflection on the tenth anniversary of Wenchuan earthquake. *Chinese Science Bulletin, 63*(19), 1865–1881. https://doi.org/10.1360/N972018-00335

Stein, R. S. (1999). The role of stress transfer in earthquake occurrence. *Nature, 402*(6762), 605–609. https://doi.org/10.1038/45144

Sun, Y., Dong, S., Fan, T., Zhang, H., & Shi, Y. (2013). 3D rheological structure of the continental lithosphere beneath China and adjacent regions. *Chinese Journal of Geophysics, 56*(9), 2936–2946. https://doi.org/10.6038/cjg20130908

Sun, Y., Luo, G., Hu, C., & Shi, Y. (2020). Preliminary analysis of earthquake probability based on the synthetic seismic catalog. *Science China Earth Sciences, 63*(7), 985–998. https://doi.org/10.1360/SSTe-2019-0117

Sun, Y., Luo, G., & Huang, L. (2021). Numerical simulation of coseismic and postseismic deformation through a node-splitting algorithm: A case study of the Wenchuan earthquake. *Journal of Geomechanics, 27*(2), 241–253. https://doi.org/10.1209/j.issn.1006-6616.2021.27.02.023

Toda, S., Lin, J., Meghraoui, M., & Stein, R. S. (2008). 12 May 2008 M=7.9 Wenchuan, China, earthquake calculated to increase failure stress and seismicity rate on three major fault systems. *Geophysical Research Letters, 35*(17), L17305. https://doi.org/10.1029/2008GL034903

Tormann, T., Enescu, B., Woessner, J., & Wiemer, S. (2015). Randomness of megathrust earthquakes implied by rapid stress recovery after the Japan earthquake. *Nature Geoscience, 8*(2), 152–158. https://doi.org/10.1038/ngeo2343

Wang, M., Shen, Z., Wang, Y., Bürgmann, R., Wang, F., Zhang, P., Liao, H., Zhang, R., Wang, Q., Jiang, Z., Chen, W., Hao, M., Li, Y., Gu, T., Tao, W., Wang, K., & Xue, L. (2021). Postseismic Deformation of the 2008 Wenchuan Earthquake Illuminates Lithospheric Rheological Structure and Dynamics of Eastern Tibet. *Journal of Geophysical Research: Solid Earth*. https://doi.org/10.1029/2021jb022399

Wang, M., Wang, F., Jiang, X., Tian, J., Li, Y., Sun, J., & Shen, Z. (2022). GPS determined coseismic slip of the 2021 Mw 7.4 Maduo, China, earthquake and its tectonic implication. *Geophysical Journal International, 228*(3), 2048–2055. https://doi.org/10.1093/gji/ggab460

Wang, Q., Qiao, X., Lan, Q., Jeffrey, F., Yang, S., Xu, C., Yang, Y., You, X., Tan, K., & Chen, G. (2011). Rupture of deep faults in the 2008 Wenchuan earthquake and uplift of the Longmen Shan. *Nature Geoscience, 4*(9), 634–640. https://doi.org/10.1038/ngeo1210

Wang, W., Cai, G., Wu, J., & Fang, L. (2023). The lithospheric S-wave velocity structure beneath the NE Tibetan Plateau and its surrounding craton basins. *Frontiers in Earth Science*. https://doi.org/10.3389/feart.2022.1066265

Wang, W., Zhao, L., Li, J., & Yao, Z. (2008). Rupture process of the Ms8.0 Wenchuan earthquake of Sichuan. *China. Chinese Journal of Geophysics, 51*(5), 1403–1410.

Wiemer, S., & Wyss, M. (2000). Minimum magnitude of completeness in earthquake catalogs: Examples from Alaska, the western United States, and Japan. *Bulletin of the Seismological Society of America, 90*(4), 859–869. https://doi.org/10.1785/0119990114

Xu, D., Xiao, J., He, J., & Wang, W. (2020). Cluster of strong earthquakes in the eastern margin of Qinghai-Tibet Plateau after Mw7.9 Wenchuan earthquake in 2008. *Science China Earth Sciences, 50*(6), 851–864. https://doi.org/10.1360/SSTe-2019-0077

Xu, X., Chen, G., Yu, G., Cheng, J., Tan, X., Zhu, A., & Wen, X. (2013). Seismogenic structure of Lushan earthquake and its relationship with Wenchuan earthquake. *Earth Science Frontiers, 20*(3), 11–20.

Xu, X., Wen, X., Yu, G., Chen, G., Klinger, Y., Hubbard, J., & Shaw, J. (2009). Coseismic reverse-and oblique-slip surface faulting generated by the 2008 Mw7.9 Wenchuan earthquake, China. *Geology, 37*(6), 515–518. https://doi.org/10.1130/G25462A.1

Zhang, S., & Zhou, S. (2016). Spatial and temporal variation of b-values in southwest China. *Pure and Applied Geophysics, 173*(1), 85–96. https://doi.org/10.1007/s00024-015-1044-7

Zhang, Y., Hu, Y., Segun, S. (2021). 3D numerical model for viscoelastic postseismic deformation following the Maule Mw8.8 earthquake in 2010. Acta Seismologica Sinica, 43(2), 180−193. https://doi.org/10.11939/jass.20200071

Zhang, Z., Yuan, X., Chen, Y., Tian, X., Kind, R., Li, X., & Teng, J. (2010). Seismic signature of the collision between the east Tibetan escape flow and the Sichuan Basin. *Earth and Planetary Science Letters, 292*(3–4), 254–264. https://doi.org/10.1016/j.epsl.2010.01.046

Zhao, B., Yang, G., Wang, J., & Dong, F. (2019). Research on b-values based on fault buffers. *Pure and Applied Geophysics, 177*(1), 71–80. https://doi.org/10.1007/s00024-019-02163-x

Zhou, R., He, Y., Ma, S., & Li, X. (1999). Late Quaternary activity characteristics of Fubianhe Fault in Sichuan's Xiaojin. *Journal of Seismological Research, 22*(4), 376–381.

Zhou, R., Li, Y., Densmore, A. L., Ellis, M. A., He, Y., Wang, F., & Li, X. (2006). Active tectonics of the eastern margin of the Tibet Plateau. *Journal of Mineralogy and Petrology, 26*(2), 40–51. https://doi.org/10.1971/j.cnki.1001-6872.2006.02.007

(Received May 16, 2023, revised September 25, 2023, accepted September 28, 2023, Published online October 12, 2023)